Instrumented drop mass for impact response measurement in stab-resistant body armour testing

S. Jenkin[1,2], B. Cazzolato[1], C.F. Jones[1] and D. Thompson[2]

[1]*School of Electrical and Mechanical Engineering, The University of Adelaide, Adelaide, 5005 South Australia, Australia,*
scott.jenkin@adelaide.edu.au
[2]*Armor Australia Pty Ltd, 126 Frederick Street, Welland, 5007 South Australia, Australia*

Abstract. The release of the Police Scientific Development Branch (PSDB) 1999 Stab Resistance Standard marked a pivotal development in stab-resistant body armour testing, introducing a rail-guided drop mass with a dual-mass design and a foam composite torso simulant. These innovations significantly improved test outcome consistency and continue to serve as the foundation for the apparatus employed in both National Institute of Justice (NIJ) Standard-0115.00 and Home Office Body Armour Standard (CAST 2017). However, factors such as the impact location on the armour panel and backing material, repeated use of damping disks, and test apparatus rigidity, are hypothesised to affect outcomes by altering the force-time and force-displacement response – collectively termed impact response. Typically, these sensitivities are inferred from penetration depth measurements, which usually require large sample sizes to identify statistically significant effects. An alternative approach that directly measures impact response using an instrumented drop mass could provide more precise assessment and a means to address these sensitivities. This paper details the development and validation of an instrumented drop mass, compliant with NIJ Standard-0115.00, designed to measure impact response in stab-resistant armour testing. Since it is not possible to directly measure the force at the threat tip, an analytical inertial compensation method was developed and experimentally validated to improve the accuracy of the estimated force transmitted to the armour. The system was used to evaluate impact responses from P1/A Edged Blade and Spike threat types on armour panels tested in accordance with NIJ Standard-0115.00. The results revealed distinct response characteristics for low- and high-penetration impacts, reflecting differences in threat geometry and penetration mechanics. This instrumented drop mass enables detailed investigation of variables influencing stab test outcomes, providing critical insights to guide future improvements in standardised apparatus and protocols, enhancing test outcome consistency within the validation of protective equipment.

1. INTRODUCTION

Stab-resistant body armour provides crucial protection against hand-delivered sharp-edged and pointed weapon attacks, for law enforcement, military and correctional personnel. Classified as life protection equipment, these armour systems must meet or exceed minimum performance requirements through standardised testing of representative samples. Modern stab testing standards, such as US National Institute of Justice (NIJ) Standard-0115.00 [1] and the UK Home Office Centre for Applied Science and Technology (CAST) Body Armour Standard, 2017 [2], evolved from foundational work outlined in UK Police Scientific Development Branch (PSDB) Stab Resistance Standard for Body Armour 1999 [3]. That earlier research led to the replacement of manual attack and air cannon launches with a rail-guided drop mass, a dual-mass configuration, and a composite foam torso simulant (backing material) to yield more consistent test outcomes that better replicate the dynamics of a hand-delivered stab impact. Although these improvements in apparatus design and protocol have enhanced repeatability compared to pre-1999 methods, several factors are still hypothesised to significantly influence test outcomes, including impact-to-edge spacing on the armour and backing material, the recovery time and number of uses of the damping disks, armour restraint, and test apparatus rigidity.

Much of the instrumented impact response testing during the PSDB 1999 development used drop towers with a single-component drop mass and backing material such as clay or gelatine, often with rigid composite or metallic armour samples [4-6]. More recently, Forster et al. [7] employed an instrumented drop mass, compliant with NIJ Standard-0115.00, to measure the acceleration response of various foam-based backing materials impacted by a circular punch, recommending stricter tolerances on density, hardness, and compression-deflection for future standards. However, published data on impact responses of modern, flexible stab-resistant armour with dual-mass drop masses and foam composite backing remains limited.

A detailed understanding of the dynamic impact response during stab testing, including forces and displacements, can provide valuable insight into the interactions between the armour panel, backing

https://doi.org/10.52202/081621-0047

material, and damping disks. This study presents the development and validation of an instrumented drop mass engineered for compliance with NIJ Standard-0115.00 and CAST 2017. Additionally, it provides typical impact response curves for both P1/A Edged Blade and Spike threat types, examining characteristic impact stages and the potential value of force-time and force-displacement data in evaluating stab-resistant armour performance.

2. EQUIPMENT

2.1 Instrumented drop mass

The instrumented drop mass (Figure 1a) is a dual-mass system with dimensions, masses, and materials compliant with both NIJ Standard-0115.00 and CAST 2017, ensuring equivalent impact energy, momentum, and configuration to conventional non-instrumented systems. To enable impact response measurement, the drop mass was instrumented with three sensors to capture uniaxial force, damping disk displacement, and acceleration.

The uniaxial force transmitted into the armour panel was measured using a custom strain gauge-based load cell, integrated with the threat holder and positioned behind the test threat along the axial load path. The load cell body, fabricated from high-tensile steel, employed a four-column design (Figure 1b). Dual-element biaxial (0°/90°) strain gauges (FCAB-5-350-11-1LJB-F, Tokyo Measuring Instruments Lab Co. Ltd., JPN) were bonded to the midspan of each column and connected in a full Wheatstone bridge configuration for single-channel force measurement (Figure 1c). The load cell was enclosed in an aluminium housing with castellation features to minimise potential off-axis bending or torsional errors in the uniaxial measurement. The load cell was calibrated by applying quasi-static compression-relaxation cycles using a universal testing machine (8874, Instron, USA) with a Dynacell (±25kN), achieving a maximum non-linearity error of 1.48% at full-scale output of 6.5 kN.

The damping disk displacement was measured using a linear potentiometer (PZ12-S-0075-L, Gefran, ITA) mounted between the threat holder and sabot. While not central to the present study, this measurement supports ongoing sensitivity analyses investigating how repeated damping disk use, including the number of impacts and recovery time, affects force-displacement behaviour and, in turn, the measured impact response at the threat-armour interface. Uniaxial acceleration was measured using an accelerometer (2264A, Endevco, USA) mounted to the sabot (Figure 1d). This was used to estimate the velocity and displacement of the sabot during impact, and, when combined with the displacement measurements from the linear potentiometer, to estimate the motion of the threat holder. The acceleration measurement also enabled inertial compensation of the measured force, as discussed in Section 2.3.

Sensor signals were recorded using an on-board data acquisition system (DAS) (SLICE NANO, Diversified Technical Systems, USA) mounted to the sabot (Figure 1e). The recorded signals were sampled at 500 kS/s, and were passed through zero-phase, 4th-order Butterworth lowpass filters with cutoff frequency adjusted by impact velocity. All instrumentation and power sources, including the sensors, DAS, and Li-ion battery, were rigidly coupled to the drop mass, forming a self-contained system without external connections or added dynamic compliance.

2.2 Stab test apparatus

Dynamic impact testing with the instrumented drop mass was conducted using an NIJ Standard-0115.00 compliant rail-guided drop apparatus (Adelaide T&E Systems, AUS) at Armor Australia's Research, Development and Engineering Facility in Adelaide, Australia (Figure 2a). The apparatus allowed precise programmatic control of impact energy up to 70 J and included an adjustable height test table, and hook-and-loop retention straps to secure the armour panel to the backing material (Figure 2b). Drop mass velocity, v_m, was determined by counting a 1 MHz clock as the sabot passed between two infrared (IR) emitter-detector pairs, spaced 50 mm apart. The table height was adjusted so that when the lowest edge of the sabot crossed the lower IR beam, the threat tip was 25 mm above the target surface, resulting in a 50 mm standoff distance, h_s. The adjusted impact energy, E_{adj}, was calculated as the sum of kinetic and potential energy associated with h_s, as shown in Equation (1), where m is the drop mass (1.902 kg) and g is gravitational acceleration. The adjusted impact velocity, v_{adj}, was then determined using Equation (2).

https://doi.org/10.52202/081621-0047

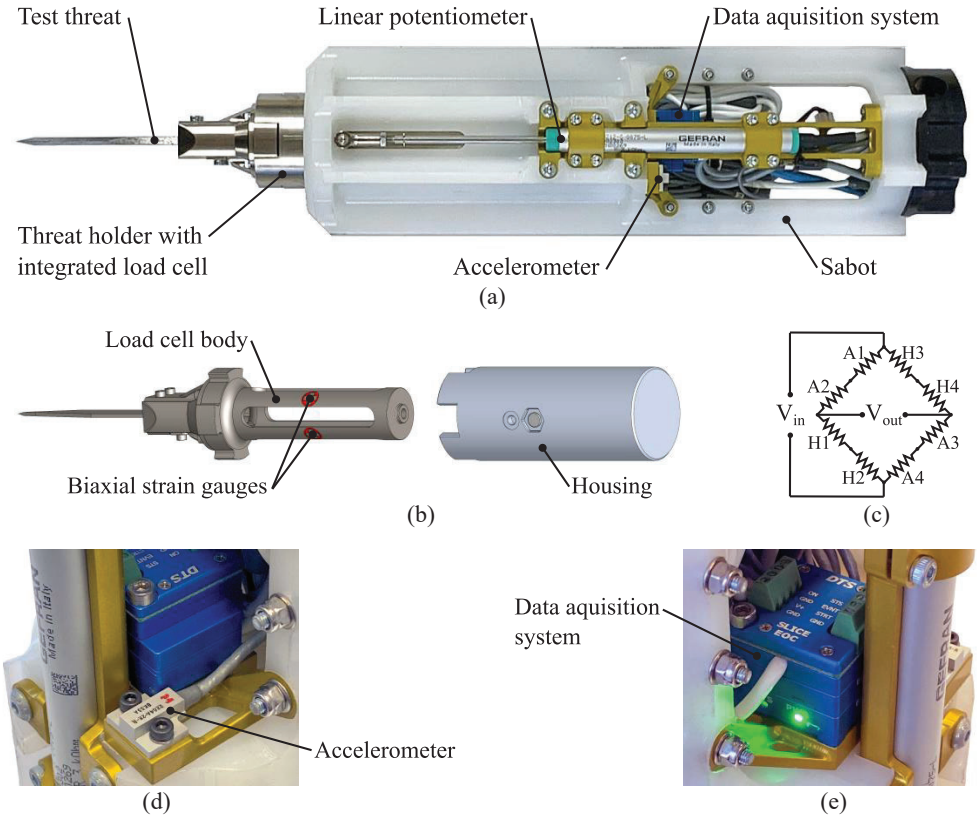

Figure 1. Instrumented drop mass: (a) front view of sabot and threat holder, (b) rendered exploded view of the threat holder with integrated load cell, (c) strain gauge wiring diagram with strain gauges A1 to A4 aligned in the axial direction and H1 to H4 aligned in the hoop direction, (d) accelerometer mounted to the sabot, and (e) data acquisition system mounted to the sabot.

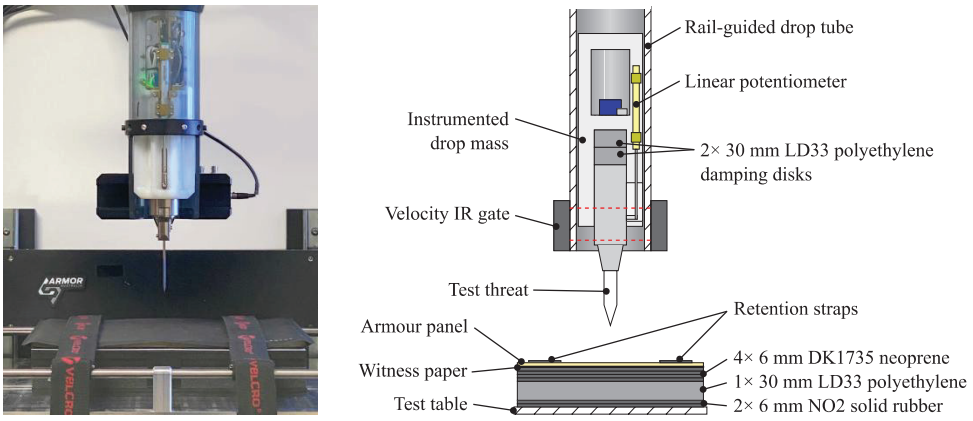

Figure 2. NIJ Standard-0115.00-compliant stab testing apparatus and experimental setup: (a) photograph of apparatus, and (b) cross-sectional schematic. The linear potentiometer in (b) is rotated 90° relative to its actual orientation in (a), to better illustrate its assembly configuration.

$$E_{adj} = \frac{1}{2} m {v_m}^2 + mgh_s \tag{1}$$

$$v_{adj} = \sqrt{\frac{2E_{adj}}{m}} \tag{2}$$

2.2.1 Test table rigidity

Test table rigidity was assessed separately from the main experimental work to facilitate comparison of apparatus used in other laboratories. Testing was conducted with NIJ-compliant backing materials, a stab-resistant armour panel, and a blunt hemispherical impactor (11 mm diameter) to replicate NIJ Standard-0115.00 conditions. A laser displacement sensor (CP24MHT80, Wenglor Sensoric, GER) was tripod mounted and physically isolated from the stab test apparatus to record deflection directly beneath the impact location. Three impacts at 24 J each resulted in maximum displacements of 0.33mm, while at 65 J, the mean maximum displacement was 0.96 mm (*SD* = 0.02 mm).

2.2.2 Backing materials and damping disks

The stab testing setup employed a multilayered backing material comprising foam and rubber layers, as specified in NIJ Standard-0115.00. The standard permits two grades each of expanded neoprene and low-density polyethylene (LDPE), which vary in mechanical properties and can significantly influence the impact response [7]. This study used DK1735 expanded neoprene and LD33 Plastazote® (Zotefoams, UK), supplied in 400 x 333 mm sheets, due to their mechanical properties closely aligning with specifications proposed by Forster et al. [7] and Draft NIJ Standard-0115.01 [8], ensuring impact responses remain relevant to both current and future standardised testing. Additionally, two 6 mm thick NO2 solid rubber sheets were placed beneath the foam backing materials. All backing materials were subjected to restitution testing in accordance with NIJ Standard-0115.00 Section 5.5.7 [1]. The rebound height of the steel sphere was determined by measuring the time of flight between its first and second bounces using an IR gate. All backing material packs satisfied the rebound height requirements of NIJ Standard-0115.00 and Draft NIJ Standard-0115.01, with a mean height of 528 mm (*SD* = 4 mm, *n* = 36).

The LD33 foam was also used for the damping disks, positioned between the threat holder and sabot (Figure 2b). The disks were precision cut to 50 mm diameter using a CNC milling machine and a custom hole saw. Table 1 details the relevant properties of all materials.

Table 1. Material properties of the backing materials.

Property	Expanded neoprene DK1735 [9]	Polyethylene foam LD33 [10]	Solid rubber NO2 [11]
Thickness (mm)	5.8-6.2	29.0-30.4 (no skin)	5.8-6.1
Density (kg/m^3)	150-200	33	1500
25% Compression Deflection (kPa)	60-90 (ASTM D1056)	66 (ISO 7214.2012)	-
50% Compression Deflection (kPa)	100-130 (ASTM D1056)	133 (ISO 7214.2012)	-
Shore Hardness	50-60 (OO)	58 (OO)	60-70 (A)

2.3 Inertial compensation of force measurement

Impact force was measured at the strain gauge location, positioned in a region of high strain uniformity but offset from the test threat tip. As a result, the measured force, F_{cell}, includes inertial contributions from the effective mass between the impact point and measurement location, and does not directly represent the forces at the threat tip, F_{tip}, or through the damping disks, F_{disk}. To estimate these quantities more accurately, an analytical inertial compensation method was developed, following an approach similar to Casem [12] for the split Hopkinson pressure bar.

2.3.1 Analytical inertial compensation method

The threat holder and load cell were analysed as a system sectioned at the strain gauge location, allowing the force components to be resolved (Figure 3a). Free-body diagrams illustrate the force interactions between the load measurement location and the threat tip (Figure 3b) and between the load measurement location and the damping disk interface (Figure 3c). The force measured by the load cell, F_{cell} is expressed in Equation (3), where $F_{inertia,th,b}$ represents the inertia force from the lower effective mass of the threat holder, $m_{th,b}$, and its acceleration, a_{th}. By incorporating the measured acceleration of the

https://doi.org/10.52202/081621-0047

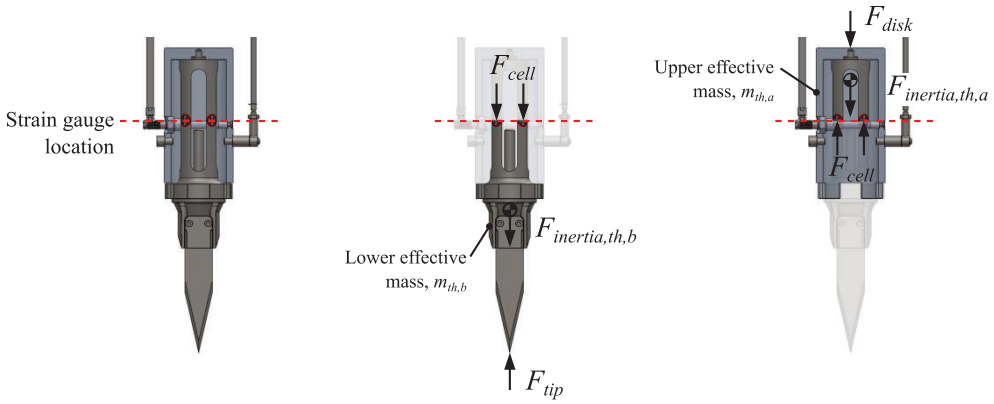

Figure 3. Rendered section view of threat holder and load cell (a) strain gauge location, (b) free-body diagram between load measurement location and threat tip, and (c) free body diagram between load measurement location and damping disk interface.

sabot, a_{sabot}, and relative displacement of the sabot and threat holder, s_{rel}, the inertia-compensated force acting at the threat tip is given by Equation (4). The sabot acceleration was first double-integrated to estimate its global displacement, which was then summed with the relative displacement from the potentiometer. The result was passed through a zero-phase, 4th-order Butterworth lowpass filter with 700 Hz cutoff frequency, before double-differentiation to remove high-frequency noise in the compensated force estimate. Similarly, the inertial compensation method was applied to estimate F_{disk}. From the free-body diagram (Figure 3c), the force balance yields Equation (5), where $m_{th,a}$ represents the upper effective mass between the strain gauge and damping disks.

$$F_{cell} = F_{tip} - F_{inertia,th,b} \tag{3}$$

$$F_{tip} = F_{cell} + m_{th,b}\frac{d^2}{dt^2}\left(\int_0^t\int_0^\tau a_{sabot}(\tau)d\tau dt + s_{rel}\right) \tag{4}$$

$$F_{disk} = F_{cell} - m_{th,a}\frac{d^2}{dt^2}\left(\int_0^t\int_0^\tau a_{sabot}(\tau)d\tau dt + s_{rel}\right) \tag{5}$$

2.3.2 Experimental validation of inertial compensation

Experimental validation of the inertial compensation method was conducted using a blunt hemispherical indenter (11 mm diameter) impacting an ultra-high molecular weight polyethylene (UHMWPE) soft armour panel with an areal density of 5.9 kg/m^2, restrained on an NIJ Standard-0115.00-compliant backing material (Figure 4). A six-axis load cell (MC5-2500, Advanced Mechanical Technology, Inc., USA) was positioned beneath the backing material to measure the transmitted force, $F_{backing}$, for comparison against the inertially compensated F_{tip}. Time alignment was performed by minimising the root-mean-square error (RMSE) between measured force signals, from initial contact to the occurrence of peak F_{tip}.

Force-time responses from five impacts at 20 J (Figure 5a) and 70 J (Figure 5b) showed that the compensated F_{tip} closely corresponded to $F_{backing}$, with differences small in magnitude and consistent in shape. The average RMSE up to peak force was 60 N for the 20 J series and 81 N for the 70 J series. These differences were primarily attributed to uncompensated inertial effects from the accelerated armour, backing material, and aluminium backplate. The consistency of these differences across all five impacts at 20 J (Figure 5c) and 70 J (Figure 5d) demonstrates that the inertial compensation method provides a reliable and accurate estimate of the force at the threat tip.

https://doi.org/10.52202/081621-0047

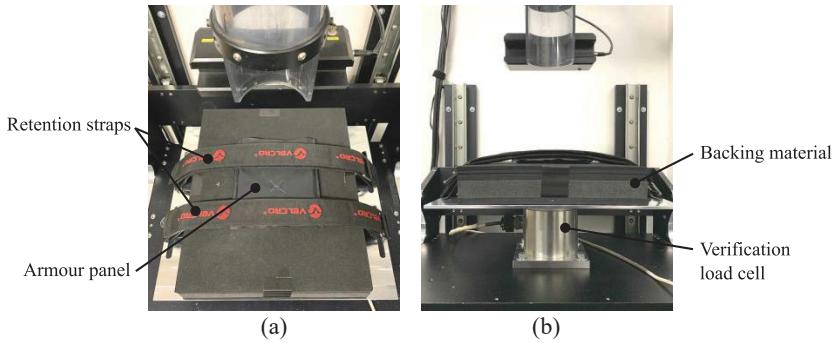

Figure 4. Experimental setup for inertial compensation validation: (a) armour panel restrained on backing material, and (b) side view of load cell mounted below the backing material.

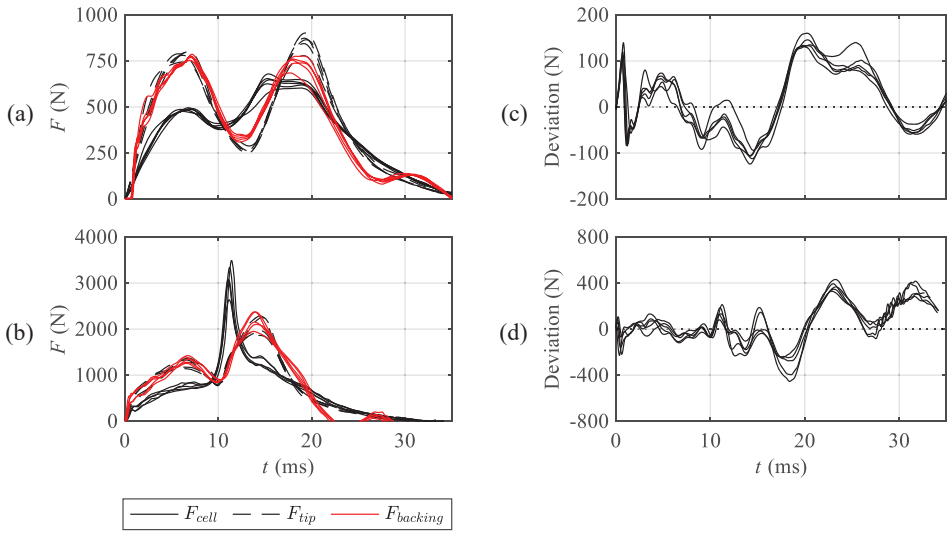

Figure 5. Experimental validation of inertial compensation method: overlay of F_{cell}, F_{tip} and $F_{backing}$ force-time responses for (a) 20 J and (b) 70 J impacts, and deviation between F_{tip} and $F_{backing}$ for (c) 20 J and (d) 70 J impacts.

3. IMPACT RESPONSE MEASUREMENT

The impact responses presented in this section were selected from a larger test series using the P1/A Edged Blade threat (n=76) and the Spike threat (n=68). While the primary objective of the larger test series was to evaluate regression methods for DOP outcomes within a novel E_{50} test methodology for stab-resistant armour [13], force-time and force-displacement responses were also recorded to characterise impact behaviour. Testing was conducted in accordance with NIJ-Standard 0115.00 on soft armour panels with a hybrid construction of para-aramid and UHMWPE fabric layers, measuring 400 x 400 mm with a total areal density of 6.7 kg/m^2. This construction meets NIJ Standard-0115.00 requirements for Edged-Blade Protection Class at Protection Level 2 and Spike Protection Class at Protection Level 1. Furthermore, the panels comply with NIJ Standard-0101.06 Level II for ballistic protection, making them representative of modern, flexible, multi-threat armour solutions used in law enforcement and security applications. Two distinct impact behaviours were observed: low-penetration impacts, where the threat did not fully penetrate the armour, and high-penetration impacts, where greater penetrative displacement between the threat and armour panel occurred.

3.1 Impact response for low-penetration impacts

Low-penetration impacts exhibited highly repeatable response curves with similar behaviour across both threat types. Force-time (Figure 6a) and force-displacement responses (Figure 6b) for a representative

https://doi.org/10.52202/081621-0047

30 J impact using the P1/A Edged Blade threat, resulting in 0 mm DOP, are presented. Corresponding acceleration, velocity, and displacement for the sabot and the threat holder are presented in Figure 6c. A consistent sequence of interactions between the test components was observed, which can be generalised into four characteristic stages of low-penetration impacts, discussed below and illustrated in Figure 6d.

Stage 0 began at the initial contact between the threat tip and the armour panel, causing rapid deceleration of the threat holder. Meanwhile, the sabot continued largely unopposed due to the low initial stiffness of the damping disks. The force at the threat tip increased linearly and reached a local peak before transitioning to Stage 1, at approximately 7 ms, when the threat holder momentarily came to rest and began to reverse direction as the sabot continued decelerating and compressing the damping disks. As the disks compressed further, they exerted increasing force until reaching a peak at Stage 2, around 14 ms. The peak damping disk compression typically exceeded 80% strain at 25 J and surpassed 90% strain at 65 J, placing them in the densification region of closed-cell foams [14]. In this region, the collapsing cell walls, elevated internal gas pressure, and compression of the bulk polymer led to a rapid rise in stress with additional strain. Consequently, the threat holder experiences peak downward acceleration into the armour, while the sabot simultaneously reached peak deceleration. Stage 3 occurred at peak threat tip force, at about 16 ms. For low-penetration impacts, the relationship between impact energy and peak threat tip force was approximately linear. From this point, the threat holder continued to displace into the backing material, while the sabot had already displaced to a global peak and had begun to reverse direction. Stage 4 is marked by the threat holder achieving its global peak displacement into the backing material, at approximately 20 ms, after which it started to recoil.

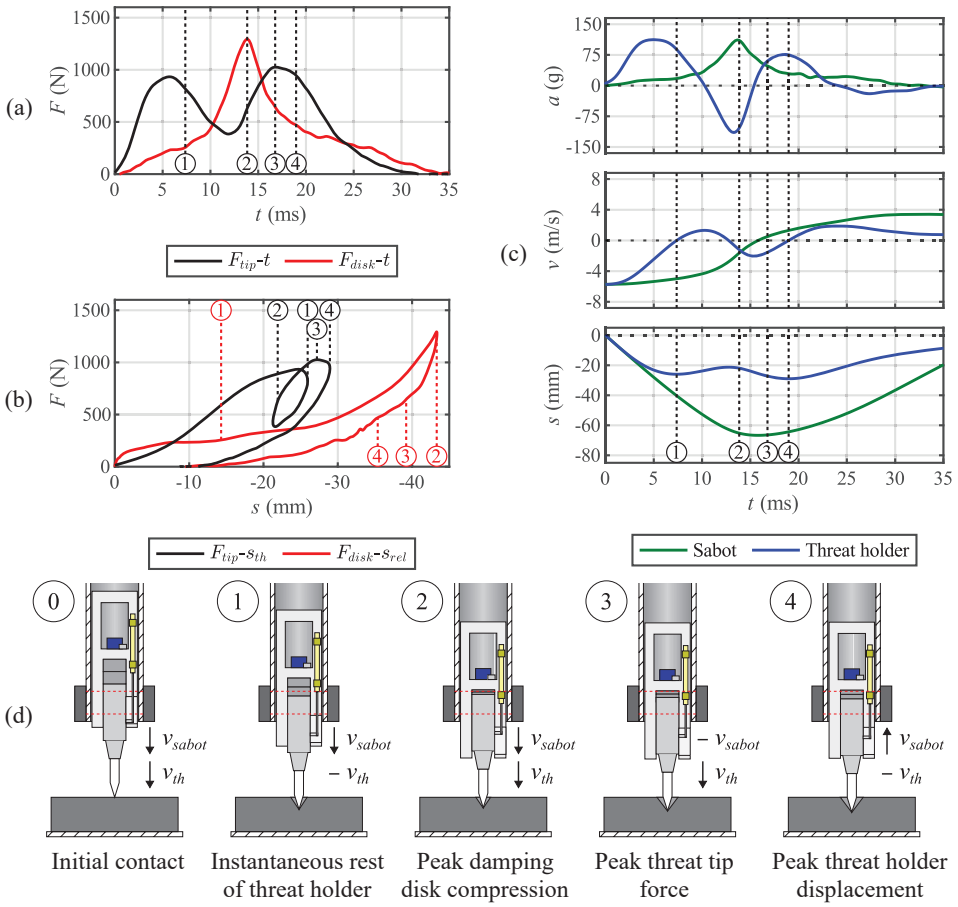

Figure 6. Impact response of a P1/A Edged Blade threat impact at 30 J (0 mm DOP) showing the characteristic stages of low-penetration impacts: (a) force-time response curves, (b) force-displacement response curves, (c) time-domain plots of acceleration (top), velocity (middle) and displacement (bottom) for both the sabot and threat holder, and (d) illustration of impact stages, indicated by encircled numbers, depicting instantaneous velocity directions of the sabot and threat holder.

3.2 Impact response for high-penetration impacts

To examine the transition from low- to high-penetration impacts, single representative impacts are presented at four energies, ranging from 30 J to 60 J for the P1/A Edged Blade threat (Figure 7) and 25 J to 55 J for the Spike threat (Figure 8). All impacts were conducted at a consistent impact location, maintaining a 94 mm impact-to-edge distance on the armour panel and 98 mm on the backing material. DOP was measured per CAST 2017 Section 7.74 [2]. For non-penetration impacts, the number of intact armour layers was counted to estimate a negative DOP using measured ply thickness. Table 2 summarises the impact response maxima and test outcomes, including the threat tip sharpness measured per NIJ Standard-0115.00 Section 5.5.5 [1], and whether the drop mass bounced out of the armour panel after impact.

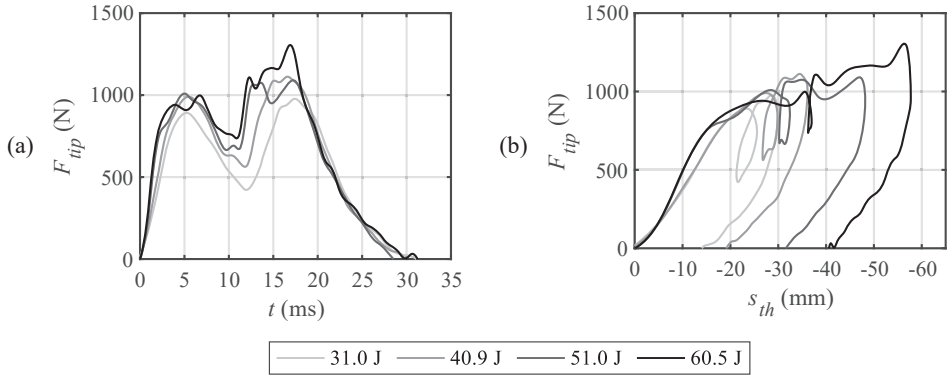

Figure 7. Impact response curves for selected single impacts using the P1/A Edged Blade threat over 31.0-60.5 J energies: (a) force-time response curves, and (b) force-displacement response curves.

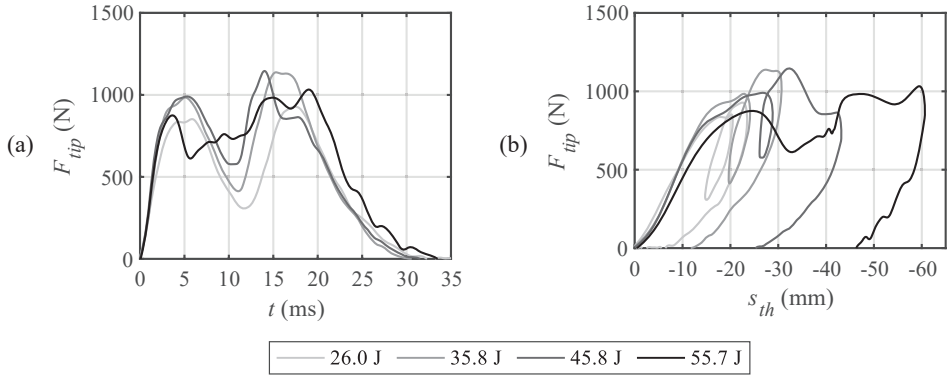

Figure 8. Impact response curves for selected single impacts using the Spike threat over 26.0-55.7 J energies: (a) force-time response curves, and (b) force-displacement response curves.

Table 2. Impact response maxima and test outcomes for selected single impacts. $F_{tip,peak}$ is the peak force at the threat tip, and $s_{th,peak}$ is the peak downward displacement of the threat holder.

E_{adj} (J)	Threat	Sharpness (HRC)	Bounce	$F_{tip,peak}$ (N)	$s_{th,peak}$ (mm)	DOP (mm)
31.0	P1/A	-139	Yes	977	-30.1	-1.3
40.9	P1/A	-142	Yes	1112	-36.1	1.8
51.0	P1/A	-123	No	1091	-48.2	14.7
60.5	P1/A	-123	Yes	1305	-57.7	21.5
26.0	Spike	-137	Yes	928	-23.5	-3.3
35.8	Spike	-132	Yes	1138	-30.7	-1.3
45.8	Spike	-141	No	1146	-43.2	10.8
55.7	Spike	-128	No	1033	-60.7	25.5

https://doi.org/10.52202/081621-0047

Impacts up to nominal 40 J for the P1/A Edged Blade, and 35 J for the Spike (shown as light grey lines in Figures 7 and 8, respectively) resulted in minimal or no penetration. Within these ranges, peak force at the threat tip increased with energy. However, once the penetration-resistance capacity of the armour was reached, further increases in energy resulted in greater threat holder displacement rather than a higher peak force. For impacts resulting in a DOP exceeding approximately 3 mm, the impact responses became more complex and exhibited greater variability compared to low-penetration impacts. The increased complexity of impact responses at higher DOP suggested that additional factors, including significant fibre cutting or parting, threat tip deformation, and friction or slippage between the threat and armour layers, introduced further variability as the threat penetrates deeper.

For the P1/A Edged Blade threat, the force-displacement curve typically exhibited a linear loading region up to approximately 20 mm displacement, followed by a penetration region where the force either plateaued or exhibited a slight increase at higher energies (Figure 7b). At 60 J, the peak force increased slightly above that observed at 50 J, suggesting that as the Edged Blade threat cuts deeper, more armour material engages, thereby increasing its penetration-resistance capacity. In contrast, the Spike threat displayed a more complex penetration phase. At 55 J, the peak force was lower than at 35 J and 45 J, particularly in the early stages (Figure 8b). This behaviour may be attributed to the slender, tapered geometry of the Spike, for which cross-sectional area increases only marginally with depth. As a result, once fibre parting occurred, the engaged armour area remained relatively unchanged as penetration progressed, limiting any further increase in penetration-resistance capacity.

Another notable trend in Figure 7a and Figure 8a was the diminishing bi-modal feature of the force-time response at the threat tip as energy increased. Deeper penetration during the early impact stages caused the threat holder to decelerate more gradually, delaying damping disk compression. Consequently, the drop mass behaved more like a single-mass system at higher DOP, reducing the distinct second force peak usually seen using a dual-mass system.

4. CONCLUSIONS

The development and validation of an instrumented drop mass marks a significant step forward in the study of stab-resistant body armour. Unlike conventional testing, which relies solely on DOP as a performance measure, the instrumented drop mass captures force-time and force-displacement responses, offering a deeper understanding of how armour materials and constructions interact with different threats under dynamic impact loading.

To improve the accuracy of force measurements at the threat tip, an analytical inertial compensation method was developed and experimentally validated. Testing with P1/A Edged Blade and Spike threats demonstrated that when DOP was small – indicating the penetration-resistance capacity of the armour was not exceeded – the impact responses were similar across both threat types and typically exhibited four characteristic stages: instantaneous rest of threat holder, peak damping disk compression, peak threat tip force, and peak threat holder displacement. However, at DOP values exceeding approximately 3 mm, impact responses became more complex, with distinct differences in force profiles and displacement behaviour observed between the threat types. For these higher DOP impacts, peak force did not directly correlate with increased DOP; instead, once the penetration-resistance capacity of the armour was reached, remaining energy was converted into further penetrative displacement.

While the instrumented drop mass is not intended to replace the drop mass currently specified in NIJ Standard-0115.00 or CAST 2017, nor is impact response intended as a certification criterion, it provides an accurate and robust method for investigating impact response within the NIJ Standard-0115.00 or CAST 2017 frameworks. The ability to measure and compare impact responses has practical applications for stab-resistant armour research and development, enabling assessments of penetration-resistance capacity, energy dissipation mechanisms, material interactions and the influence of layering strategies, all under normal test conditions. These insights can contribute to the development of more advanced armour constructions, ultimately enhancing personal protection against Edged Blade and Spike threats.

Beyond armour material and state-of-the-art stab-resistant armour solution development efforts, the instrumented drop mass is currently being used in sensitivity analyses to investigate factors hypothesised to contribute to test outcome variability. These include impact location on both the armour

and backing material, the recovery time and repeated use of damping disks, armour restraint, test apparatus rigidity and variations in backing material properties. By systematically evaluating these variables, identifying those with greatest influence, and implementing appropriate controls, the instrumented drop mass has the potential to improve test outcome consistency, strengthening the foundation of standardised evaluation methods for stab-resistant armour systems.

Acknowledgments

This research was supported by the Australian Government through the Department of Education's National Industry PhD Program (project 36179). The views expressed herein are those of the authors and are not necessarily those of the Australian Government or the Department of Education.

References

[1] NIJ Standard 0115.00, Stab Resistance of Personal Body Armor, National Institute of Justice, September 2000.
[2] Payne T., O'Rourke S. and Malbon C., Home Office Body Armour Standard (2017), CAST publication number 012/17, July 2017.
[3] Pettit M. and Croft J., PSDB stab resistance standard for body armour, PSDB publication number 6/99, 1999.
[4] Horsfall I., Stab resistant body armour, PhD thesis, Cranfield University, March 2000.
[5] Chadwick E., Nicol A., Lane J. and Gray T., Biomechanics of knife stab attacks, Forensic Science International, 105 (1999), 35-44.
[6] Nicol A., Chadwick E. and Gray T., Investigation of knife stab characteristics – development of body tissue simulant, Technical report, University of Strathclyde, Scottish Executive Central Research Unit, 1998.
[7] Forster A.M., Chan-Ou-Teung A. Guigues E. Forster A.L., Davis J. and Rice K., Foam composite specifications and qualification in support of NIJ 0115.00, Personal Armour Symposium Proceedings 2014, Cambridge UK.
[8] Draft NIJ Standard 0115.01, Stab resistance of body armour, National Institute of Justice, March 2020.
[9] Alanto Ltd, Specification Sheet, DK1735 Expanded Neoprene Sponge Rubber, Issue 2, 2015.
[10] Alanto Ltd, Specification Sheet, LD33 – Low Density Polyethylene Foam, Issue 1, 2018.
[11] Alanto Ltd, Specification Sheet, NO2 Commercial Economy Solid, Issue 1, 2016.
[12] Casem D., Weerasooriya T. and Moy P., Inertial effects of quartz force transducers embedded in a plot Hopkinson pressure bar, Experimental Mechanics, 45, 368-376.
[13] Jenkin S., Cazzolato B., Jones C.F. and Thompson D., E50 testing for stab-resistant body armour evaluation, Personal Armour Symposium Proceedings 2025, Bruges BEL.
[14] Gibson L., Modelling the mechanical behaviour of cellular materials, Materials Science and Engineering: A, 110 (1989), 1-36.

https://doi.org/10.52202/081621-0047